DOI: 10.1002/adma.200601830

RuO_2 Nanowires and RuO_2/TiO_2 Core/Shell Nanowires: From Synthesis to Mechanical, Optical, Electrical, and Photoconductive Properties**

By *Yu-Lun Chueh*, *Chin-Hua Hsieh, Mu-Tung Chang*, *Li-Jen Chou*,* *Chang S. Lao*, *Jin H. Song*, *Jon-Yiew Gan*, and *Zhong L. Wang**

Functional 1D metal oxides have attracted much attention because of their unique applications in electronic, optoelectronic, and spintronic devices.[1] For semiconducting oxide nanowires (NWs) (e.g., ZnO, In_2O_3, and SnO_2 NWs), field-effect transistors and light-emitting diodes have been demonstrated.[2] Metallic oxide nanoscale materials, such as nanoscale RuO_2, can be good candidates as interconnects in electronic applications.[3] RuO_2 nanomaterials have been produced by chemical vapor deposition (CVD) and through chemical reaction.[3b,4] Recently, RuO_2 NWs have been synthesized using pure Ru as metal target under different flux ratios of O_2/Ar in a reactive sputtering system.[5]

For core/shell structures, extensive research has been carried out on systems such as Ge/Si,[6] GaN/AlN/AlGaN,[7] Ta_2O_5/SiO_2,[8] and Fe_3O_4/MgO.[9] The Ge/Si core/shell NW, for example, is a high-performance field-effect transistor because of the reduced carrier scattering. GaN/AlN/AlGaN core/shell NWs exhibit a high electron mobility. For the SiO_2/Ta_2O_5 core/shell structure, the axial confinement of light propagation can effectively reduce the energy loss owing to the difference in refractive index between Ta_2O_5 and SiO_2.

Following the successful synthesis of a RuO_2/TiO_2 core/shell structure by reactive sputtering,[10] we mainly focus on the investigation of the physical properties of the RuO_2 NWs in the present study. The detailed epitaxial relationship and electronic structures of the RuO_2/TiO_2 core/shell structure synthesized by reactive sputtering are investigated. The mechanical, optical, and electrical properties and photocatalyst response to UV irradiation are characterized. Our results suggest the potential application of the NWs as interconnects and optoelectronic devices.

Figure 1a shows a scanning electron microscopy (SEM) image of RuO_2 NWs synthesized by the reactive sputtering approach at a synthesis temperature of 450 °C for 3 h, and indicates a high density of uniform RuO_2 NWs more than several micrometers long. In addition, most of the RuO_2 NWs have a square cross section, as shown in the inset of Figure 1a. The corresponding X-ray diffraction (XRD) spectrum, shown in Figure 1b, confirms that the phase of the NWs is rutile-structured RuO_2 with lattice-constant values of $a = 0.45$ nm and $c = 0.31$ nm. After deposition of a thin TiO_2 layer via reactive sputtering deposition, the morphology of these NWs remains unchanged, but the sizes increase, as shown in Figure 1c. The corresponding XRD spectrum of the NWs is shown in Figure 1d. It is hard to distinguish if the individual peaks originate from either RuO_2 or TiO_2 owing to the fact that the lattice mismatch between RuO_2 and TiO_2 is less than 5 %.

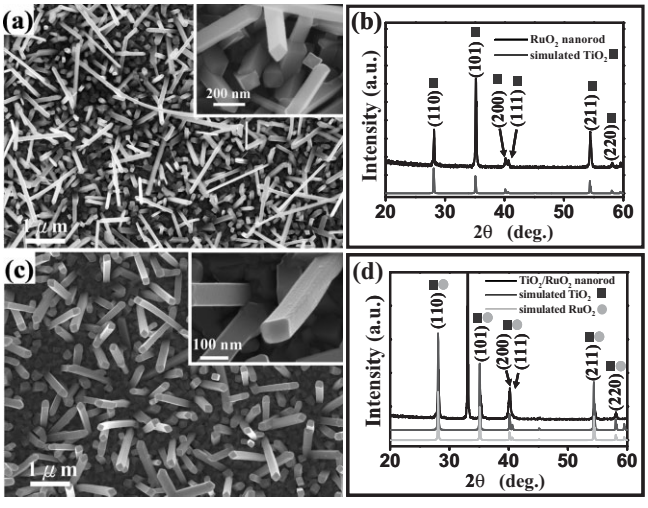

Figure 1. a) SEM image of RuO_2 NWs synthesized by reactive sputtering at 450 °C for 3 h. The inset shows a magnified SEM image of RuO_2 NWs. b) XRD spectrum of the RuO_2 NWs. The marked spectrum shows the simulated result. c) SEM image of the RuO_2/TiO_2 core/shell structure. The inset shows the corresponding magnified SEM image. d) XRD spectrum of the RuO_2/TiO_2 core/shell structure. The marked spectra represent the simulated results.

[*] Prof. L.-J. Chou, Dr. Y.-L. Chueh, C.-H. Hsieh, M.-T. Chang, Prof. J.-Y. Gan
Department of Materials Science and Engineering
National Tsing-Hua University
Hsinchu, Taiwan 300 (ROC)
E-mail: ljchou@mx.nthu.edu.tw
Prof. Z. L. Wang, Dr. Y.-L. Chueh, C. S. Lao, J. H. Song
School of Materials Science and Engineering
Georgia Institute of Technology
Atlanta, GA 30332-0245 (USA)
E-mail: zhong.wang@mse.gatech.edu

[**] This research was supported by the National Science Council through Grant No. NSC 94-2215-E-007-019, the Thousand Horse Program No. 095-2917-I-007-014, NSF, the NASA Vehicle System Program, Department of Defense Research and Engineering (DDR&E), the Defense Advanced Research Project Agency (N66001-040-1-18903), and CCNE from NIH. Supporting Information is available online from Wiley InterScience or from the author.

ADVANCED MATERIALS

Figure 2a shows a transmission electron microscopy (TEM) image of a RuO_2 NW with a diameter of 105 nm. The corresponding diffraction pattern with the [110] zone axis is shown in the inset of Figure 2b, indicating the [001] growth direction (*c*-axis). From the high-resolution TEM (HRTEM) image, shown in Figure 2b, two *d* values of 0.32 and 0.31 nm, which are consistent to the $(1\bar{1}0)$ and (001) planes, respectively, can be found. In addition, the average diameter of the RuO_2 NWs, obtained from examining an ensemble of RuO_2 NWs via TEM, is ca. 105 nm (see Fig. S1a in the Supporting Information for a statistical analysis).

A TEM image of a RuO_2 NW shelled with a TiO_2 layer is shown in Figure 2c, where two distinctly different image contrasts can be found. Figure 2d shows a HRTEM image taken from the interface between TiO_2 and RuO_2, and the inset in Figure 2d shows the corresponding diffraction pattern. The epitaxial relationship between rutile TiO_2 and RuO_2 is $(110)_{TiO_2} \| (110)_{RuO_2}$ and $[1\bar{1}0]_{TiO_2} \| [1\bar{1}0]_{RuO_2}$, However, some mismatch dislocations can be found at the interface between TiO_2 and RuO_2, captured by selecting the symmetric $\pm(1\bar{1}0)$ diffraction beams using Fourier filtering. Three edge dislocations are created very close to each other within $(1\bar{1}0)$ planes (Fig. S2) owing to the 5 % lattice mismatch.[11] The average diameter of the RuO_2/TiO_2 core/shell NWs is 165 nm (Fig. S1b).

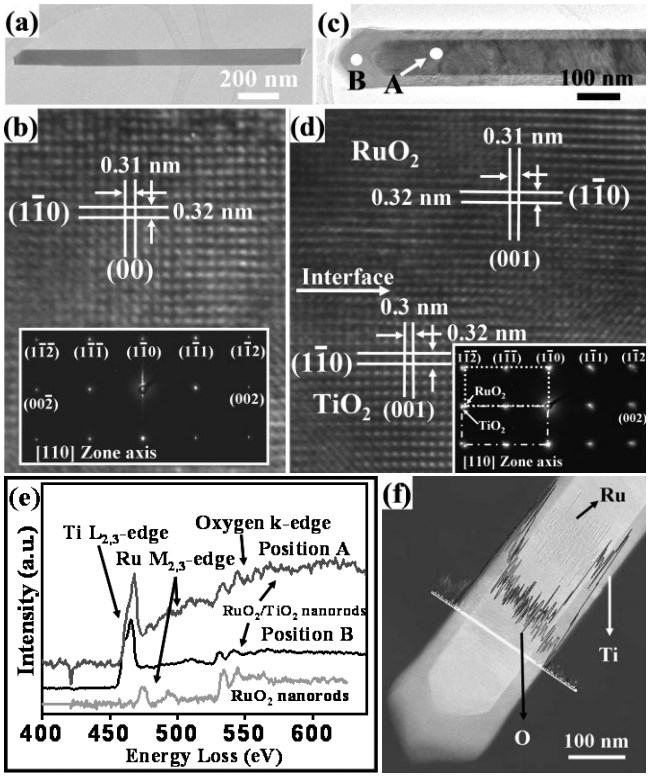

Figure 2. a) TEM image of a RuO_2 NW with a diameter of 105 nm. b) The corresponding high-resolution TEM image. Two *d*-spacings of 0.32 and 0.31 nm are identified, which is consistent with the $(1\bar{1}0)$ and (001) planes, respectively. The inset shows the diffraction pattern with [110] zone axis, indicating that the growth direction of RuO_2 is along [001]. c) TEM image of a RuO_2/TiO_2 core/shell structure with a diameter of 160 nm. d) HRTEM image of the RuO_2/TiO_2 core/shell structure taken from the interface between TiO_2 and RuO_2. The corresponding *d*-spacings and planes are indexed and identified. The inset shows the diffraction pattern of which the two matrixes deviated from TiO_2 and RuO_2 are displayed. e) EELS spectrum for the Ti L-edge and O K-edge ELNEFS of the RuO_2/TiO_2 core/shell structure recorded from two points, labeled A and B for the RuO_2 core and the TiO_2 shell, respectively. The bottom EELS spectrum was acquired from a RuO_2 NW as reference. f) The corresponding HAADF image of a RuO_2/TiO_2 core/shell structure. The distribution of Ru, Ti, and O are shown.

The electronic and chemical structures of the NWs were examined by electron energy loss spectroscopy (EELS), which is sensitive to the unoccupied valence band. All the raw data acquired by EELS have been calibrated in an energy scale by the zero-loss peak and deconvoluted by the low-loss region to reduce the multiple-scattering effect. Figure 2e shows the EELS spectra recorded from selected positions (labeled with A and B for the RuO_2/TiO_2 core/shell structure in Fig. 2c). For comparison, the EELS spectrum shown at the bottom of Figure 2e was taken from a RuO_2 NW without a TiO_2 coating. For the EELS from the TiO_2 shell (position B), Ti $L_{2,3}$-edge and O K-edge energy loss near edge fine structure (ELNES) is clearly found. In the spectrum acquired from position A, the Ru M-edge is present. The EELS results indicate the presence of the core/shell structure. Figure 2f shows the high-angle annular dark-field (HAADF) microscopy image for this RuO_2/TiO_2 core/shell structure with the corresponding EDS line scan. The image contrasts and different element distribution across the whole NW confirm the core/shell structure.[12]

By using an atomic force microscopy (AFM) instrument in contact mode, the elastic modulus of the NWs was measured without destroying the sample by using a technique developed by Song et al.[13] In the present study, a tetrahedral Si-tip was used as cantilever with a calibrated normal spring of 1.76 $N\,m^{-1}$ (AC240TS, Asylum Research), and the lateral spring constant (K_L) can be calculated by $K_L = W^2 K_n / T^2$, where *W*, *T*, and K_n represent the width and thickness of the cantilever, and the normal force spring constant, respectively. The set point (constant normal force) and scanning speed are maintained at 100 nN and 7 $\mu m\,sec^{-1}$. The overall behavior of the NWs in contact-mode scanning is schematically illustrated in Figure 3a–d.[13] Both the topography image (the signal from the feedback of scanner) and the lateral-force image were recorded simultaneously, and are shown in Figure 3e and f for RuO_2 NWs and in Figure 3g and h for the RuO_2/TiO_2 core/shell structure. The scanning area was set as 10×10 μm. The bright tails found in the lateral-force images (Fig. 3f and g) are a result of the deflection of the nanowires along the scanning direction, as pushed by the tip. As a result, the length of the NWs and the elastic modulus for each individual RuO_2 NW can be estimated as ca. 1.669–3.205 μm and ca. 113–390 GPa, respectively, by taking the average length and radius of the NWs presented in Table 1. The average elastic modulus is about 250 GPa, which is consistent with the bulk value of 249–313 GPa.[14] The RuO_2 NWs have a higher elastic modulus than other NWs, for example, SiC (610–660 GPa),[15] ZnO (29–230 GPa),[13,16] GaN (227-305 GPa),[17] and Si (93–250 GPa).[18]

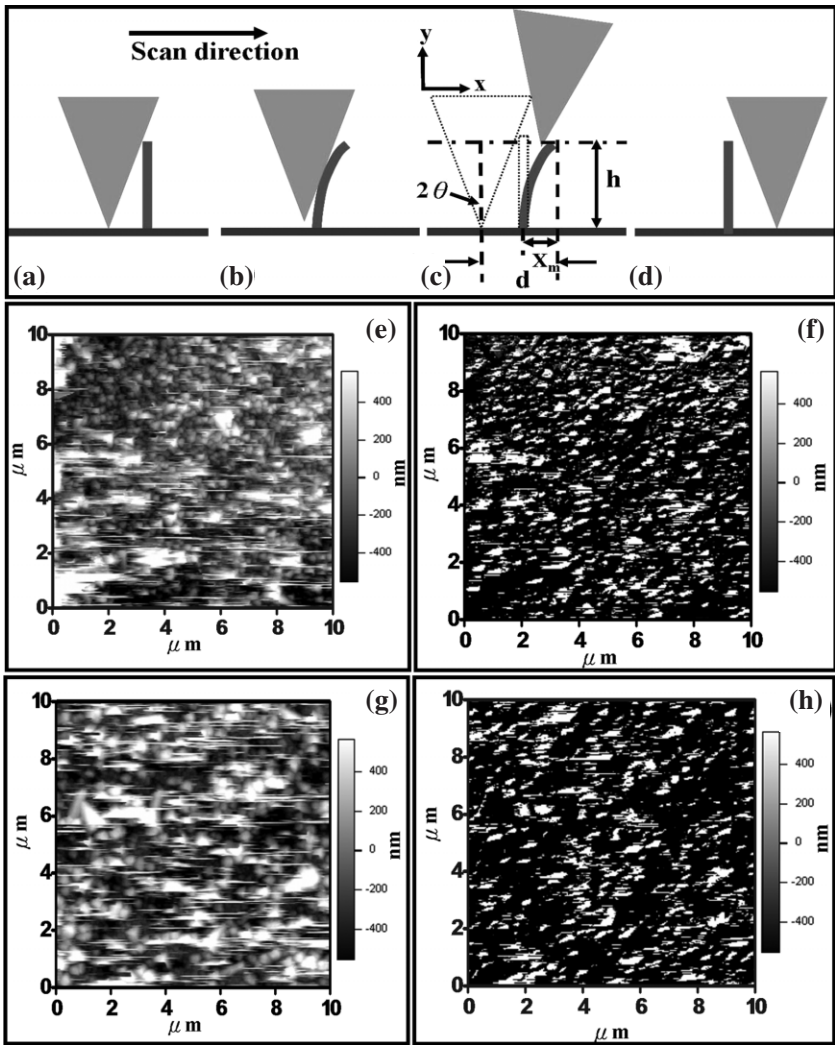

Figure 3. a–d) Schematic illustration of AFM tip scanning across a NW. e,f) The topography and lateral-force images of the RuO_2 NWs, respectively. g,h) The topography and lateral-force images of RuO_2/TiO_2 core/shell structure, respectively.

Table 1. The elastic modulus of RuO_2 and the RuO_2/TiO_2 core/shell structure measured by AFM.

RuO_2 NWs	Length [μm]	Elastic modulus [GPa]	RuO_2-TiO_2 coaxial NWs	Length [μm]	Elastic modulus [GPa]
1	2.068	169	1	1.936	177
2	2.513	390	2	2.088	250
3	2.593	143	3	1.721	221
4	2.268	330	4	1.895	90
5	2.319	304	5	2.086	446
6	2.305	249	6	2.055	91
7	3.271	233	7	1.661	123
8	1.697	113	8	1.374	91
9	3.205	161	9	1.398	130
10	1.987	416	10	1.825	424
11	2.077	209	11	2.306	196
12	1.669	261	12	1.878	90

For the RuO_2/TiO_2 core/shell structure, the elastic modulus is in the range 90–424 GPa, as presented in Table 1. The average elastic modulus is found to be about 194 GPa. However, in comparison with the average elastic modulus of the RuO_2 NWs, the elastic modulus of the RuO_2/TiO_2 core/shell structure is found to have decreased by ca. 22 %. The decrease of the elastic modulus can be accounted for by the composite of RuO_2 and TiO_2. Based on flexural rigidity as theory for transverse deflection, EI can be defined as the effective flexural rigidity of the core/shell structure, for which E represents the effective elastic modulus of that core/shell structure. Hence, an effective elastic modulus can be given, without considering shear deformation, as[16]

$$EI = E_c I_c + E_s I_s \quad (1)$$

where E_c and E_s represent the elastic moduli of the core and the shell, respectively, and the variables $I_c = a^4/12$ and $I_s = (b^4 - a^4)/12$ are the cross-sectional moments of inertia for the core and the shell, respectively. The values a and b represent the diameters of the RuO_2 core and the total RuO_2/TiO_2 core/shell structure, respectively, using a cylindrical geometrical approximation. By taking the average bulk elastic modulus for both the RuO_2 core ($E_c = 281$ GPa) and the TiO_2 shell ($E_s = 200.5$ GPa), along with average values for a and b of ca. 105 nm and ca. 165 nm, respectively, the effective modulus of the core/shell structure with a TiO_2-shell thickness of ca. 25 nm is found to be ca. 208 GPa, in reasonable agreement with the measured result.

The photoluminescence (PL) spectrum is a simple and useful tool to find optoelectronic applications of the RuO_2/TiO_2 core/shell structure. The PL measurements were performed at room temperature using a He–Cd laser with a wavelength of 325 nm, and the PL signal was amplified by a photomultiplication tube (PMT). However, no PL spectrum can be obtained from the RuO_2 NWs due to their metallic character, by which the conduction and valence bands almost overlap by partial occupation of the Ru 4d states.[19] On the other hand, a peak at 809 nm (1.53 eV) and a broad peak (2–3.5 eV) are found for the RuO_2/TiO_2 core/shell structure, as shown in Figure 4. The inset in Figure 4 shows the Gaussian-fitted result of the spectrum. Peaks located at 388 nm (3.2 eV), 426 nm (2.9 eV), and 488 nm (2.5 eV) are found. The emission peak at 388 nm (3.2 eV) is larger than the transition from the band-edge emission of 3.03 eV for TiO_2.[20] Similar results have

ADVANCED MATERIALS

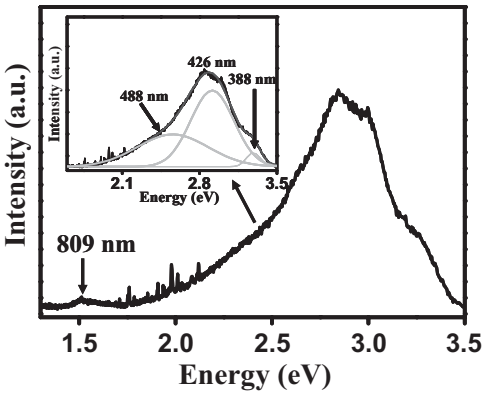

Figure 4. The photoluminescence (PL) spectrum for the RuO_2/TiO_2 core/shell structure excited at 326 nm at room temperature. Inset: Gaussian fit.

been reported in the literature, and it is suggested that this is due to quantum confinement.[21] However, the size of our NWs is much larger than the dimensions required to have a quantum size effect. In addition, our findings in the PL spectrum are consistent with previous results by Wu et al.,[22] where four peaks at 418 nm (3 eV), 465 nm (2.7 eV), 536 nm (2.3 eV), and 834 nm (1.5 eV) were found for rutile TiO_2 nanowires, except that in our study a blue-shift of ca. 30–50 nm (0.1–0.2 eV) is found by scrutinizing all the PL peaks in detail. This blue-shift may be caused by the stress and surface-resonance effects introduced by the lattice mismatch (2–5 %) between RuO_2 and TiO_2 (the lattice constants of which are $a = 0.4494$ nm, $c = 0.31071$ nm and $a = 0.4593$, $c = 0.2959$ nm, respectively) and the high surface-to-volume ratio of the RuO_2/TiO_2 core/shell structure.[23] From the TEM image, shown in Figure 2d, the TiO_2 shell undergoes a tensile stress along [001] (*c*-axis) and a compress stress along both [100] and [010] (*a*-axis), which may enlarge the bandgap of TiO_2, resulting in the blue-shift of the peaks. A similar result can be found for SiC NWs, for which the bandgap will be monotonically increased as the tensile stress is applied along the axial direction.[24] In other materials, such as GaN thin films, the stress caused by different atom sizes resulting from doping of foreign atoms can enlarge the bandgap, resulting in a blue-shift in the PL spectrum as well.[25] On the other hand, the origin of the peak at 388 nm (3.2 eV) is attributed to self-trapped excitons located at TiO_6 octahedral sites, an intrinsic property found at both rutile and anatase structures.[22,26] In addition, the peaks at 426 nm (2.9 eV) and 488 nm (2.5 eV) are caused by absorption of oxygen atoms on the surface that can capture electrons to create shallow traps as radiative or nonradiative centers (F, F^+, and F^{++}).[27] The peak at 809 nm (1.52 eV) is ascribed to Ti^{3+} interstitial ions, which are associated with the oxygen vacancies by removal of a neutral oxygen bridge in the basic rutile cell, in which each Ti^{4+} ion is surrounded by six O^{2-}, resulting in a slightly disordered octahedron.[28]

RuO_2 NWs may be potential candidates for interconnects in circuit applications. To characterize the *I–V* characteristics, a NW was aligned between two Au electrodes via the dielectrophoresis technique and Pt was deposited as the top electrode to make a perfect contact by focused ion beam (FIB) microscopy.[1,29] A LabView program was used to control the *I–V* testing process. Although the electron affinity of RuO_2 (4.87 eV) is smaller than the work function of Pt (5.6 eV), a linear fit was found in the *I–V* diagram as shown in Figure 5a. This is probably a result of the metallic behavior of RuO_2 NWs.[3a,30] By examining several different *I–V* curves of RuO_2 NWs, the resistance was found to be in the range of 0.4–1.2 kΩ at room temperature (Fig. S3). In addition, the resistivity of these RuO_2 NWs was measured to be 215–640 μΩcm by taking the diameters and lengths of the RuO_2 NWs (as provided by SEM observation) into account, which is consistent with the reported resistivity of 40–482 μΩcm for a RuO_2 thin film.[19,31]

The results of durability and reliability tests of the RuO_2 NW were obtained by performing *I–V* measurements under a higher applied voltage, as shown in Figure 5b. The NW can

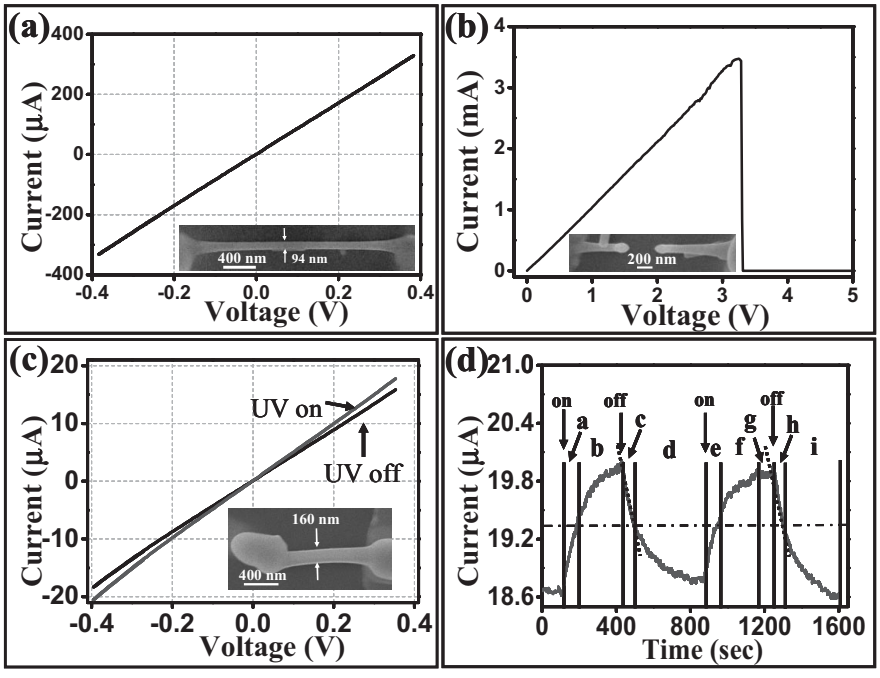

Figure 5. a) *I–V* curve for a RuO_2 NW at room temperature. b) The *I–V* curve recorded at a high applied voltage. c) The *I–V* curve for RuO_2/TiO_2 core/shell structure with and without UV illumination. d) The current as a function of the UV illumination time.

endure a current of up to 3.3 mA before failure, corresponding to a current density of 4×10^7 A cm^{-2}. The failure point occurs in the middle of the NW, as shown in the inset of Figure 5b. The possible reason for failure is self-heating, which is consistent with NiSi, $TaSi_2$, and FeSi metallic NWs.[32] In comparison to other nanowires, such as NiSi NWs (3×10^8 A cm^{-2}),[32a] carbon nanotubes (CNTs) (10^9 A cm^{-2}),[33] $TaSi_2$ (3×10^8 A cm^{-2}),[32b] FeSi (1.6×10^7 A cm^{-2}),[32c] and Pd NWs (2×10^6 A cm^{-2}),[34] the current-density carried by RuO_2 NWs is reasonably good. It is therefore possible for it to be used as an interconnect.

The photocatalyst behavior of TiO_2 has been extensively studied because it can catalytically decompose volatile compounds under UV light.[35] It is well known that thinner NWs may further enhance the sensitivity of the devices owing to an increased surface-to-volume ratio. Here, we investigate the photoconductivity of the RuO_2/TiO_2 core/shell structure under UV illumination of 256 nm (4.9 eV), which is strong enough to excite the electron–hole pair near the band edge. For the photoconductivity measurements, all the devices were excited by UV light with a wavelength of 256 nm. The contact metal used in this study was Pt with a work function of 5.6 eV, which is smaller than the work function of TiO_2 (7.3 eV), so that the contact between the Pt electrode and TiO_2 is ohmic.[36] The corresponding *I–V* curve without UV illumination (obtained via two terminal probes measurements) shown in Figure 5c, demonstrates a linear behavior, confirming the ohmic contact feature. The inset in Figure 5c shows an SEM image of the RuO_2/TiO_2 core/shell structure with a diameter of 160 nm and a length of 1.5 μm. As a result, the effective resistivity of the NW at room temperature is calculated as ca. 0.044 Ω cm (Fig. S4), which is much smaller than that of pure thin-film TiO_2 (2 MΩ cm).[37] The resistivity decreases to 0.032 Ω cm after the UV light has been turned on for 8 min. In addition, the *I–V* curve as a function of UV illumination time is shown in Figure 5d, where the externally applied voltage along the NW was fixed at 0.4 V, and the individual UV on/off response times are presented in Table 2. The current of the RuO_2/TiO_2 core/shell structure rapidly increased from 18.5 μA to 19.4 μA within 88 s (area a) and then slowly increased to get a saturated current of 20 μA within 219 sec (area b) during the first illumination with UV light. After the UV light was turned off, the current drastically decreased from 20 μA to 19.4 μA within 52 s (area c) and then decreased very slowly to the original (dark-current) value within 385 s (area d). The second illumination with UV light was performed to confirm the previous results. The current quickly increased from 18.5 μA to 19.4 μA within 87 s (area e) and started to reach the saturated value of 20 μA within 222 s (area f) after the second time the UV light was turned on. The UV light was kept on for 101 sec (area g) so that a maximum current plateau of 20 μA was maintained. After the UV light was turned off, the current quickly dropped from 20 μA to 19.4 μA within 47 s (area h) and returned to its original (dark-current) value within 350 s (area i). In general, TiO_2 can be considered as an n-type semiconductor, which is caused by the oxygen deficiencies.[38] However, the surface-adsorption of water molecules can terminate the oxygen deficiencies (vacancies) on the surface of TiO_2 by a physisorption process followed by a chemisorption process to form hydroxyl bonding (OH^-), which retards the transport of electrons inside the TiO_2 if the nanowire is exposed to the atmosphere.[39] In addition, the oxygen molecules can capture the electrons and terminate the oxygen vacancies as well.[40] Both water and oxygen molecules can form the space-charge region (SCR), i.e., the depletion region that influences the conductance in such a manner that the conduction and valence bands near the surface of the TiO_2 shell are bent upward.[37] Once electron–hole pairs are generated by UV light near the band edge of TiO_2, they can proceed in two possible distinct processes: removal of adsorbed oxygen species (O_2, O^{2-}, and O_2^-) and water species (H_2O, OH^-) in the SCR, and increasing the net carrier density, thus enhancing the conductance.

It is worth noting that the current decay rate (52 s for the first illumination and 47 s for the second illumination) is faster than the current increment rate (88 s for the first illumination and 87 s for the second illumination). This is due to the fact that the water and oxygen molecules are very fast to adsorb to and accumulate on the surface via physisorption and chemisorption because of the larger surface-to-volume ratio, resulting in a drastic drop in conductance as the UV light was turned off. This fast adsorption can be confirmed by PL spectra where the highest intensity of peaks at 426 nm (2.9 eV) results from the shallow traps (F, F^+, and F^{++}) caused by adsorption of oxygen atoms on the surface (Fig. 4). Once the number of oxygen defect sites on the surface of the TiO_2 shell has gradually decreased, the extra molecules have to diffuse much deeper into the TiO_2 shell to find available oxygen defect sites, and capture more electrons.[40,41] As a result, this diffusion behavior of the adsorbent will become the dominant reaction process to slow down the whole adsorption process. This is why the decay of the current via adsorption is fast at first and then becomes much slower (385 and 350 s after the first and second UV illuminations are turned off).

However, it should be noted that the surface barrier caused by adsorption can be suppressed when the nanowire size reaches a critical diameter due to the strong effect from surface states, resulting in slightly less band bending.[42] Consequently, it can be expected that an SCR should be created within the whole TiO_2 shell to suppress the surface-barrier height (less band upward on the surface) caused by adsorption

Table 2. The different photoresponse times for the individual time periods a–i (Fig. 5) after the 1st and 2nd UV illumination.

Action	Response time [s]								
	a	b	c	d	e	f	g	h	i
1st UV on/off	88	219	52	385					
2nd UV on/off					87	222	101	47	350

ADVANCED MATERIALS

of foreign molecules due to the fact that the average thickness of the TiO_2 shell is about 25 nm. This can enhance the probability of recombination between photogenerated electron–hole pairs and foreign adsorbed molecules to increase the conductance when the UV light is on. Once most of the molecules are removed, the probability for adsorption via physisorption and chemisorption by extra foreign molecules on the TiO_2 surface will gradually increase because a reaction between the clear surface and foreign molecules is more favorable. The desorption by photogenerated electron–hole pairs and adsorption by foreign molecules needs to be balanced, resulting in a slowly saturated current.[41]

In summary, we have investigated the microstructure and electronic structure of RuO_2 NWs and RuO_2/TiO_2 core/shell structure NWs using HRTEM and EELS. The TiO_2 layer is epitaxially grown on the surface of the RuO_2 NWs, and exhibits the same crystal orientation as the RuO_2 NWs. The elastic modulus of the RuO_2 NWs was measured to be 113–390 GPa using AFM. The elastic modulus of the RuO_2/TiO_2 core/shell structure NWs can be understood based on an effective medium model. The PL analysis of the RuO_2/TiO_2 core/shell structure indicates its potential for applications in optoelectonics. For RuO_2 NWs, the resistance at room temperature was found to be 0.4–1.2 kΩ with a resistivity of 215–640 $\mu\Omega$cm. In addition, the maximum current density before failure was measured to be 4×10^7 A cm^{-2}. Furthermore, the photoconductivity of the RuO_2/TiO_2 core/shell structure under UV light has been studied. Our research indicates that the RuO_2-based NWs are good and relevant candidates for interconnects and optoelectronics.

Experimental

For the NW growth, single-crystal (001) Si wafers (1–30 Ω cm) were cleaned by the standard cleaning process. SiO_2 layers with a thickness of 200 nm are formed on the Si substrate. Reactive sputtering was used to grow RuO_2 NWs under the growth conditions of various gas mixture of Ar and O_2 at synthetic temperatures of 200–500 °C, a pressure of 10^{-2} Torr (1 Torr = 1.333×10^2 Pa) and a radiofrequency power of 20 W. For the synthesis of the RuO_2/TiO_2 core/shell structure, the TiO_2 layer was sputtered onto the surface of RuO_2 NWs with a gas mixture of Ar (10 sccm) and O_2 (10 sccm), and the rf power of 20 W at annealing temperature of 450 °C for 30 min.

The surface morphology was examined by a field-emission scanning electron microscope (JSM-6500F), operated at 15 kV. For TEM study, the samples were sonicated in ethanol and then dispersed in copper grid supported by a holey carbon film. A field-emission TEM instrument (JEM-3000F) operated at 300 kV with a point-to-point resolution of 0.17 nm and equipped with an energy dispersion spectrometer (EDS) and an electron energy loss spectrometer (EELS), was used to characterize the microstructures and chemical compositions.

Received: August 10, 2006
Revised: October 10, 2006
Published online: December 12, 2006

[1] a) C. S. Lao, P. X. Gao, L. Zhang, D. Davidovic, R. Tummala, Z. L. Wang, *Nano Lett.* **2006**, *6*, 263. b) J. Zhou, S. Z. Deng, L. Gong, Y. Ding, J. Chen, J. X. Huang, J. Chen, N. S. Xu, Z. L. Wang, *J. Phys. Chem. B* **2006**, *110*, 102 916. c) A. Ponzoni, E. Comini, G. Sberveglieri, J. Zhou, S. Z. Deng, N. S. Xu, Y. Ding, Z. L. Wang, *Appl. Phys. Lett.* **2006**, *88*, 203 106.

[2] a) T. H. Moon, M. C. Jeong, B. Y. Oh, M. H. Ham, M. H. Jeun, W. Y. Lee, J. M. Myoung, *Nanotechnology* **2006**, *17*, 2116. b) J. M. Bao, M. A. Zimmler, F. Capasso, X. W. Wang, Z. F. Ren, *Nano Lett.* **2006**, *6*, 1719. c) P. Nguyen, H. T. Ng, T. Yamada, M. K. Smith, J. Li, J. Han, M. Meyyappan, *Nano Lett.* **2004**, *4*, 651. d) Y. R. Ryu, T. S. Lee, J. A. Lubguban, H. W. White, Y. S. Park, C. J. Youn, *Appl. Phys. Lett.* **2005**, *87*, 153 504. e) S. V. Kalinin, J. Shin, S. Jesse, D. Geohegan, A. P. Baddorf, Y. Lilach, M. Moskovits, A. Kolmakov, *J. Appl. Phys.* **2005**, *98*, 044 503.

[3] a) R. Sahul, V. Tasovski, T. S. Sudarshan, *Sens. Actuators, A* **2006**, *125*, 358. b) C. Ducati, D. H. Dawson, J. R. Saffell, P. A. Midgley, *Appl. Phys. Lett.* **2004**, *85*, 5385.

[4] C. S. Hsieh, D. S. Tsai, R. S. Chen, Y. S. Huang, *Appl. Phys. Lett.* **2004**, *85*, 3860.

[5] Y. T. Lin, C. Y. Chen, C. P. Hsiung, K. W. Cheng, J. Y. Gan, *Appl. Phys. Lett.* **2006**, *89*, 1.

[6] J. Xiang, W. Lu, Y. G. Hu, Y. Wu, W. Yan, H. Yan, C. M. Lieber, *Nature* **2006**, *441*, 489.

[7] Y. Li, J. Xiang, F. Qian, S. Gradčak, Y. Wu, H. Yan, D. A. Blom, C. M. Lieber, *Nano Lett.* **2006**, *6*, 1468.

[8] Y. L. Chueh, L. J. Chou, Z. L. Wang, *Angew. Chem. Int. Ed.* **2006**, in press.

[9] D. Zhang, Z. Liu, S. Han, C. Li, B. Lei, M. P. Stewart, J. M. Tour, C. Zhou, *Nano Lett.* **2004**, *4*, 2151.

[10] K. W. Cheng, Y. T. Lin, C. Y. Chen, C. P. Hsiung, J. Y. Gan, J. W. Yeh, C. H. Hsieh, L. J. Chou, *Appl. Phys. Lett.* **2006**, *88*, 043 115.

[11] P. X. Gao, Y. Ding, W. J. Mai, W. L. Hughes, C. S. Lao, Z. L. Wang, *Science* **2005**, *309*, 1700.

[12] V. Grillo, E. Carlino, *Ultramicroscpoy* **2006**, *106*, 603.

[13] J. H. Song, X. D. Wang, E. Riedo, Z. L. Wang, *Nano Lett.* **2005**, *5*, 1954.

[14] a) S. K. Hong, H. J. Kim, H. G. Yang, *J. Appl. Phys.* **1996**, *80*, 822. b) J. S. Tse, D. D. Klug, K. Uehara, Z. Q. Li, J. Haines, J. M. Le'ger, *Phys. Rev. B: Condens. Matter Mater. Phys.* **2000**, *61*, 10 029.

[15] E. W. Wong, P. E. Sheehan, C. M. Lieber, *Science* **1997**, *277*, 1971.

[16] C. Q. Chen, Y. Shi, Y. S. Zhang, J. Zhu, Y. J. Yan, *Phys. Rev. Lett.* **2006**, *96*, 075 505.

[17] C. Y. Nam, P. Jaroenapibal, D. Tham, D. E. Luzzil, S. Evoy, J. E. Fischer, *Nano Lett.* **2006**, *6*, 153.

[18] a) M. Tabib-Azar, M. Nassirou, R. Wang, S. Sharma, T. L. Kamins, M. S. Islam, R. S. Williams, *Appl. Phys. Lett* **2005**, *87*, 113 102. b) S. Hoffmann, I. Utke, B. Moser, J. Michler, S. H. Christiansen, V. Schmidt, S. Senz, P. Werner, U. Gösele, C. Ballit, *Nano Lett.* **2006**, *6*, 662.

[19] J. J. Lin, W. Xu, Y. L. Zhang, J. H. Huang, Y. S. Huang, *Phys. Rev. B: Condens. Matter Mater. Phys.* **1999**, *59*, 344.

[20] J. J. We, C. C. Yu, *J. Phys. Chem. B* **2004**, *108*, 3376.

[21] a) J. M. We, H. C. Shih, W. T. Wu, *Nanotechnology* **2006**, *17*, 105. b) D. Maestre, A. Cremades, J. Piqueras, *Nanotechnology* **2006**, *17*, 1584.

[22] J. M. Wu, H. C. Shih, W. T. Wu, Y. K. Tseng, I. C. Chen, *J. Cryst. Growth* **2005**, *281*, 384.

[23] a) Joint Committee on Powder Diffraction Standards, JCPDS card No. 43-1027. b) JCPDS card No. 34-0180. c) C. W. Chen, K. H. Chen, C. H. Shen, A. Ganguly, L. C. Chen, J. J. Wu, H. I. Wen, W. F. Pong, *Appl. Phys. Lett.* **2006**, *88*, 241 905. d) H. Shalish, H. Temkin, V. Narayanamurti, *Phys. Rev. B: Condens. Matter Mater. Phys.* **2004**, *69*, 245 401. e) H. M. Kim, D. S. Kim, D. Y. Kim, T. W. Kang, Y. H. Cho, K. S. Chung, *Appl. Phys. Lett.* **2003**, *81*, 2193.

[24] B. Yan, G. Zhou, W. H. Duan, J. Wu, B. L. Gu, *Appl. Phys. Lett.* **2006**, *89*, 023 104.

[25] G. Popovic, G. Y. Xu, A. Botchkarev, W. Kim, H. Tang, A. Savador, H. Morkoc, R. Strange, J. O. White, *J. Appl. Phys.* **1997**, *82*, 4020.

[26] a) H. Tang, H. Berger, P. E. Schmid, F. Levy, *Solid State Commun.* **1993**, *87*, 847. b) L. V. Sarat, S. I. Patil, S. B. Ogle, S. R. Sainker, S. T. Kshirsager, *Int. J. Mod. Phys. B* **1998**, *12*, 2635.

[27] a) *Luminescence and Related properties of II–IV Semiconductors* (Eds: D. R. Vij, N. Singh), NOVA Science Publishers, Commack, NY **1998**, p.320. b) Y. Lei, L. D. Zhong, G. W. Meng, G. H. Li, X. Y. Zhang, G. H. Li, X. Y. Zhang, C. H. Liang, W. Chen, S. X. Wang, *Appl. Phys. Lett.* **2001**, *78*, 1125.

[28] a) R. Plugaru, A. Cremads, J. Pigueras, *J. Phys.: Condens. Matter* **2004**, *16*, S261. b) I. Ferna'ndez, A. Cremades, J. Piqueras, *Semicond. Sci. Technol.* **2005**, *20*, 239.

[29] a) P. A. Smith, C. D. Nordquist, T. N. Jackson, T. S. Mayer, B. R. Martin, J. Mbindyo, T. E. Mallouk, *Appl. Phys. Lett.* **2000**, *77*, 1399. b) L. Shi, Q. Hao, C. H. Yu, D. Kim, N. Mingo, X. Y. Kong, Z. L. Wang, *Appl. Phys. Lett.* **2004**, *84*, 2638.

[30] C. S. Hsieh, D. S. Tsai, R. S. Chen, Y. S. Huang, *Appl. Phys. Lett.* **2004**, *85*, 3860.

[31] W. D. Ryden, A. W. Lawson, *Phys. Rev. B: Condens. Matter Mater. Phys.* **1970**, *1*, 1494.

[32] a) Y. Wu, J. Xiang, C. Yang, W. Lu, C. M. Lieber, *Nature* **2004**, *430*, 61. b) Y. L. Chueh, M. T. Ko, L. J. Chou, L. J. Chen, C. S. Wu, C. D. Chen, *Nano Lett.* **2006**, *6*, 1637. c) A. L. Schmitt, M. J. Bierman, D. Schmeisser, F. J. Himpsel, S. Jin, *Nano Lett.* **2006**, *6*, 1617.

[33] Z. Yao, C. L. Kane, C. Dekker, *Phys. Rev. Lett.* **2000**, *86*, 2941.

[34] C. Cheng, R. K. Gonela, Q. Gu, D. T. Haynie, *Nano Lett.* **2004**, *5*, 175.

[35] a) A. L. Insebigler, G. Lu, J. T. Yates Jr., *Chem. Rev.* **1995**, *95*, 735. b) J. Lin, J. C. Yu, D. Lo, S. K. Lam, *J. Catal.* **1999**, *183*, 368.

[36] a) S. Kaji, T. Nakayama, J. Yamauchi, *J. Phys.: Conf. Ser.* **2006**, *29,* 120. b) A. Kiejna, T. Pabisiak, S. W. Gao, *J. Phys.: Condens. Matter* **2006**, *29*, 120.

[37] K. Pomoni, A. Vomvas, C. Trapalis, *Thin Solid Films* **2005**, *479*, 160.

[38] S. D. Yoon, Y. Chen, A. Yang, T. L. Goodrich, X. Zuo, D. A. Arena, K. Ziemer, C. Vittoria, V. G. Harris, *J. Phys.: Condens. Matter* **2006**, *18*, L355.

[39] a) S. E. Ahm, J. S. Lee, H. Kim, S. Kim, B. H. Kang, K. H. Kim, G. T. Kim, *Appl. Phys. Lett.* **2004**, *84*, 5022. b) X. Feng, L. Feng, M. Jin, J. Zhai, L. Jiang, D. Zhu, *J. Am. Chem. Soc.* **2004**, *126*, 62. c) R. D. Sun, A. Nakajima, T. Fujishima, T. Wantanabe, K. Hashimoto, *J. Phys. Chem. B* **2001**, *105*, 1984.

[40] S. Kim, J. Maier, *Electrochem. Solid State Lett.* **2003**, *6*, J7.

[41] K. Vanheusden, W. L. Warren, C. H. Seager, D. R. Tallant, J. A. Voigt, B. E. Gnade, *J. Appl. Phys.* **1996**, *79*, 7983.

[42] R. Calarco, M. Marso, T. Richter, A. L. Aykanat, R. Meijers, A. F. D. Hart, T. Stoica, H. Lüth, *Nano Lett.* **2005**, *5*, 981.

